National Aeronautics and Space Administration

FINAL TECHNICAL REPORT
FOR NASA GRANT NAGW-1370

Submitted to:

National Aeronautics and Space Administration
Technical Officer, Code EZ
NASA Headquarters
Washington, DC 20546

Submitted by:

The Trustees of Columbia University
in the City of New York
Box 20, Low Memorial Library
New York, New York 10027

Prepared by:

Columbia Astrophysics Laboratory
Departments of Astronomy and Physics
Columbia University
538 West 120^{th} Street
New York, New York 10027

Title of Research:

"Development of a High Resolution Liquid Xenon Imaging Chamber for Gamma-Ray Astronomy"

Principal Investigator:

Elena Aprile
Associate Professor of Physics

Period Covered by Report:

1 May 1988 – 30 April 1990

Final Technical Report for NASA Grant NAGW-1370

Elena Aprile, Principal Investigator

1. INTRODUCTION

The NASA grant NAGW-1370 was award to partially support a research program entitled "Development of a High Resolution Liqud Xenon Imaging Chamber for Gamma-Ray Astronomy," under the direction of Professor Elean Aprile at the Columbia Astrophysics Laboratory.

The objective of the research was to develop the technology of LXe detectors for spectroscopy and imaging of γ-rays from astrophysical sources emitting in the low to medium energy regime. In particular the technical challenges and the physical processes relevant to the realization of a LXe detector operated as a Time Projection Chamber (TPC) were addressed and studied.

Experimental results have been obtained on the following topics:

1) Long distance drift of free electrons in LXe (Purity).
2) Scintillation light yield for electrons and alphas in LXe (Triggering).
3) Ionization yield for electrons and gamma-rays in LXe (Energy Resolution).

In the following we summarize the major results from the above investigations. For more details we refer to the papers which have so far been accepted or submitted for publication in refereed journals.

2. RESEARCH ACCOMPLISHMENTS

2.1. Long Distance Drift of Free Electrons in LXe (Purity)

The purity of liquid xenon is a key issue for the successful operation of a liquid xenon ionization TPC. The presence of electronegative impurities in the liquid leads to the capture of the free electrons thus reducing the available signal and the energy resolution. One of the goals of the proposed research was to build a gas purification and liquification system and to test the liquid xenon purity with a measurement of the electrons lifetime before capture by impurities. We have fulfilled that objective and the conclusions reached by us are presented in the following. For a more detailed report we refer to Aprile *et al.* (1991 (A)).

2.1.1. The LXe Purity Monitor

A gridded ionization chamber with a drift gap of 6 cm and an active volume of about 1 liter was used to conduct the studies on liquid xenon purity. Cosmic rays traversing the chamber generated electrons which drifted towards the anode under the influence of an external electric field. To be sensitive to the effect of electron attachment by electronegative impurities, long drift paths or equivalently long drift times were achieved by reducing the electric field strength. Data were recorded for electric fields in the range 7V/cm to

500V/cm. From a pulse shape analysis of the signals induced on the anode by the drifting electrons, information on the electron lifetime and thus on the total impurity concentration was obtained.

Figure 1 shows a shematic view of the purity monitor and the associated electronics and triggering system used for the electron lifetime measurements. The cathode and anode of the gridded ionization chamber were stainless steel discs of diameters 5.9 cm and 4.0 cm, respectively. The grid was an electroformed nickel mesh with a shielding efficiency of about 99%. The collection field to drift field ratio was fixed to 3 to ensure 100% transmission of the electrons. To maintain a uniform electric field in the drift region, field shaping rings were introduced between the cathode and the grid. The whole electrode assembly, held together by ceramic spacers, was suspended from the top flange of the chamber vessel. Negative HV was supplied to the grid, cathode and field shaping rings from an external divider chain via a multiple feedthrough. A separate feedthrough was used to readout the anode signal.

Figure 2 shows a schematic of the purification and gas handling system developed by us. Commercial grade xenon was transferred into a 1 gallon stainless steel high pressure cylinder which acted as the gas reservoir in all our experiments. Prior to filling, the cylinder was ultrasonically cleaned and evacuated and baked out at 200°C for 24 hours.

In its purification cycle, the xenon gas first passed through a commercial Oxisorb to reduced the O_2 concentration below 0.1 ppm by chemisorption and the water concentration below 0.5 ppm. Next the gas passed through a molecular sieve trap at room temperature containing about 1 kg of 4A type synthetic zeolites to remove molecules with an effective diameter of less than 4A. These include water, CO_2 and light hydrocarbons. Finally, the xenon gas was passed through two high temperature getters. The materials for the two getters were alloys of Zr-V-Fe and Zr-Fe, respectively. Before the gas filling, both the getters were activated at 350°C for 2 hours. After the activation, the two getters were maintained at the operational temperatures of 500°C and 150°C, respectively, during the entire gas filling period. The regeneration of the molecular sieve filter after each passage of the gas was accomplished by baking at a temperature of 350°C under a good vacuum. We found that approximately four cycles of purification were necessary to bring the commercial gas to the desired level of purity.

The entire system used stainless steel pipes and the connections were either welded or made with high vacuum fittings. The valves were all metal bakeable ones.

The purified gas was liquified in the chamber surrounded by a cryogenic bath of freon 11 and dry ice. This mixture was particularly convenient since it provided a stable temperature of 195 K throughout the entire data taking period. At this temperature the xenon vapour pressure is about 4 atm. To maintain a steady flow, the gas was passed through the purifiers at a pressure of about 5 atm. The entire system was built to withstand pressures of about 10 atm. After each measurement, the xenon gas was recuperated into the stainless steel reservoir, kept in a liquid N_2 bath.

A charge sensitive preamplifier was connected to the anode to detect the electron component of the ionization signal poduced by the cosmic rays. A digital oscilloscope (Tektronix 2430A) was used to digitize the signal. The waveforms were then transferred to a Macintosh computer, from which they were transferred to a micro-Vax computer for

further analysis.

2.1.2. The Method of Pulse Shape Analysis

The lifetime of the electrons before capture by electronegative substances is a function of the liquid purity and can be determined from an analysis of the measured waveforms.

The number, N_0, of electron-ion pairs generated by a cosmic ray traversing through the chamber is estimated to be about 1.5×10^5, using the relation

$$N_0 = (dE/dx)_{\min} \cdot L/W, \tag{1}$$

where $(dE/dx)_{\min}$ is the specific ionization for minimum ionizing particles in LXe (3.9 MeV/cm), L is the drift distance (6 cm) and W is the average energy to create an electron-ion pair (15.6 eV).

The electrons which escape initial recombination, drift toward the anode with a drift velocity v_d and induce a charge signal $Q(t)$ on the anode only after they cross the grid. The charge signal at time t is given by:

$$Q(t) = \int_0^t eNv_d/Ldt = eNt/t_d. \tag{2}$$

Here e is the electron charge, N is the number of electrons that survive recombination, and t_d is the drift time, $t_d = L/v_d$.

If electronegative impurities (X) are present in the liquid xenon, a certain fraction of electrons will be captured before reaching the anode, forming heavier electronegative ions (X^-):

$$e + X \rightarrow X^-. \tag{3}$$

The attachment rate constant k for the reaction is given by

$$k = \int_o^\infty \sigma(v) f(v, E) dv. \tag{4}$$

Here v is the electron agitation velocity, $f(v, E)$ is the electron velocity distribution, E is the applied electric field and $\sigma(v)$ is the attachment cross-section to the impurity of type X. Since the number of electrons lost per unit time through the attachment process can be expressed by

$$dN/dt = -k[X]N(t) \tag{5}$$

the number of conduction electrons remaining at time t is given by

$$N(t) = Ne^{(-t/\tau)} \tag{6}$$

where τ, the average electron lifetime before capture is related to the impurity concentration $[X]$ by

$$\tau = \frac{1}{k[X]}. \tag{7}$$

The equation for the induced charge is then modified to

$$Q(t) = (eNt/t_d)(1 - e^{(-t/\tau)}) \quad \text{for} \quad 0 < t < t_d. \tag{8}$$

To analyze the data the observed pulses were fitted with the equation

$$V_{\text{out}}(t) = \int_0^t Q(k)R(k-t)dk, \tag{9}$$

where the response function, $R(t)$, of the electronics is taken into account. $R(t)$ is obtained from the response of the electronics to a known test pulse.

2.1.3. Attenuation Length of Ionization Electrons in LXe

Figure 3 shows ionization pulses taken at different electric fields. The superimposed solid curve is the best fit to the data using equation (9). The full transit time which is in excess of 200 μsec is still visible at the lowest field. Figure 4 shows the fitted electron lifetimes as a function of electric field. The error bars correspond to a 90% confidence level. Within errors, the data are consistent with a constant electron lifetime in excess of 220 μsec.

The oxygen equivalent concentration of impurities in liquid xenon is estimated by using equation (7). With 220 μsec for the electron lifetime as deduced from our data, 2×10^{11} liter/moles/sec for the attachment rate constant (Bakale *et al.* 1976), $n = 21$ for the number of moles in one liter of liquid xenon at temperature $T = 195$ K we obtain:

$$[X] \leq 1 \text{ ppb (oxygen equivalent)}.$$

The drift velocity at different electric fields was determined from the measurement of the drift times and the known drift distance. This method is applicable only for the cases where the lifetime of the drifting electrons is much longer than the drift time. In our case this is true to the lowest field. The graph of drift velocity against the electric field is shown in Fig. 5. Our results are very much consistent with the data obtained by other groups as shown in the figure. At 500V/cm the drift velocity approaches a value of about 2 mm/μsec. Using the relation

$$v_d = \mu E \tag{10}$$

and fitting the data in the linear region (for fields less than 30 V/cm) we obtain the value of low field mobility at the temperature of 195K to be

$$\mu_o = 4230 \pm 400 \text{ cm}^2\text{V}^{-1}\text{s}^{-1}. \tag{11}$$

Using this low field mobility, the attenuation length of electrons before capture is deduced to be 44 cm, considerably larger than the maximum drift length planned for the liquid xenon imaging TPC under developement.

2.2. Scintillation Light of Electrons and Alpha Particles in LXe

Liquid xenon is not only an excellent ionizer but also an excellent scintillator with an efficiency comparable to that of NaI(Tℓ).

The detection of the fast (< 5 nsec) light signal associated with any γ-ray event in the sensitive volume will provide an ideal trigger for the readout system of the TPC.

Liquid xenon scintillates in the vacuum ultraviolet region (160 nm – 190 nm). This scintillation process is attributed to the radiative de-excitation of excimers. The excimers can be formed in liquid xenon either through the excitation process or through the recombination process associated with the ionizing particle. The scintillation originated from the excitation process is called the excitation luminescence and that from the recombination process is called the recombination luminescence.

One can reduce the recombination luminescence by applying an electric field preventing the electrons from recombining with the positive ions. Since the electric field has to be strong enough to sweep the electrons out of the ionization track before they are captured by the ions, the field strength to quench the recombination luminescence depends strongly on the electron ion density in the ionization track. For excitation associated with minimum ionizing particles, the recombination luminescence can be completely quenched at an applied electric field of about 2 kV/cm, while only 5% of the recombination luminescence is eliminated even at 10 kV/cm for alpha particle excitation.

In the electron excitation case, one can observe the time profile of the excitation luminescence under the complete quenching condition. It shows a fast decay component and a slow decay component, since the excimers can populate the $^1\Sigma_u^+$ and $^3\Sigma_u^+$ states having the decay times of 5 nsec and 30 nsec, respectively. When no electric field is applied, the recombination luminescence is superimposed over the excitation luminescence. Since the recombination process is relatively slow when it is associated with electron excitation because of the low electron-ion density along the ionization track, the scintillation signal is less sharp than that with an applied electric field.

In the alpha particle excitation case, the complete suppression of the recombination luminescence is not attainable under practical electric field strengths. Since the recombination process, however, proceeds much faster than the de-excitation process, the scintillation time profile is governed by the de-excitation process. The apparent time profile is, therefore, similar to the excitation scintillation time profile of the electron excitation case with an enhancement of the fast component due to the selective production of the $^1\Sigma_u^+$ state through the recombination process.

2.2.1. LXe Scintillation Test Chamber

In order to investigate the expected characteristics of the liquid xenon scintillation discussed above, as well as its correlation with the collected charge , we used a parallel plate ionization chamber as shown in Fig. 6 (Aprile *et al.* 1990 (B)). A honeycomb mesh with an optical transmission of 78% was used as anode in order to have an effective optical coupling. To examine the ionization density effect on the scintillation signal we used an ^{241}Am alpha source and a ^{207}Bi internal conversion electron source, electroplated on the center of the cathode. When tested with the electron source, the chamber was provided

with a shielding grid. The scintillation light emitted in liquid xenon was detected with an UV sensitive photomultiplier (Hamamatsu R2059), optically coupled to the chamber through a CaF_2 window. The UV photomultiplier was operated at the Freon-dry ice temperature (195K) to reduce the thermal emission of electrons from the photocathode.

The ionization signal on the anode was detected with a charge sensitive amplifier having a sensitivity of 1 volt/pC. The charge pulses were fed into a shaping amplifier with an optimized differential and integral time constants of 3μsec, and then analyzed with a multichannel analyzer (Canberra 35Plus).

To examine the time correlation between charge and light, the shaped pulses were also observed with a digital oscilloscope (Tektronix 2430A) triggered with the scintillation signal. The photomultiplier anode was terminated with a 50Ω resistor to trace the time profile of the scintillation on the digital oscilloscope, while the dynode was terminated with a 500 kΩ resistor to have an output amplitude proportional to the scintillation intensity. The dynode pulses were delivered to a shaping amplifier with differential and integral time constants of 0.25μsec and 5μsec, respectively, and were observed with the oscilloscope triggered by the anode signal.

The chamber was evacuated for over 48 hours before each measurement, attaining an ultimate vacuum better than 1.0×10^{-7} torr and an outgas rate less than 1×10^{-9} torr$\cdot\ell$/sec. We followed the same gas handling and purification procedure as described in the previous section to supply ultra-clean liquid xenon to the chamber.

2.2.2. Time Dependence of the LXe Scintillation Light

Figure 7 (a) and (b) show the averaged anode pulse of the photomultiplier corresponding to the time dependence of the scintillation of liquid xenon excited by electrons without and with an applied electric field of 2kV/cm, respectively. As explained above, the scintillation light consists of a fast component with a decay time shorter than 5 nsec and a slow component with a decay time of 30 nsec, in good agreement with previously reported values (Kubota *el al.* 1982).

Figure 8 (a) and (b) show the averaged anode pulse of the photomultiplier corresponding to the time dependence of the scintillation in liquid xenon excited by alpha particles without and with an applied electric field of 7.9kV/cm. By comparison with Fig. 8 (b), it is clearly seen that the fast component is enhanced in the alpha particle excitation and that the time dependence of the scintillation is hardly affected by the applied electric field in the observed time scale.

Since the rise time of the photomultiplier t_{pm} is 1.3 nsec, one could estimate the rise time of the scintillation light t_s to be 2.1 nsec, by using the relation $t_{ob}^2 = t_s^2 + t_{pm}^2$. The decay time is governed by the radiative deexcitation process of the xenon excimers produced in liquid xenon by alpha particles as explained before. The apparent decay time of 15 nsec has been interpreted as a composition of two different decay times of 4 nsec and 27 nsec, corresponding to the lifetimes of two different excited states ($^1\Sigma_u^+, ^3\Sigma_u^+$) of the excimers (Kubota *et al.* 1982).

Since the specific ionization density significantly affects the time dependence of the scintillation light of liquid xenon as we described, it is possible to distinguish the electron events associated with gamma-rays from those produced by heavier ionizing particles

by using pulse shape discrimination. This will provide an effective background rejection mechanism.

Figure 9 shows the shaped dynode pulse of the photomultiplier, triggered with the photomultiplier anode pulse in the case of alpha particle excitation. The dynode pulse height is proportional to the scintillation intensity in liquid xenon excited by the alpha particles. Figure 10 (a) and (b) show the ^{241}Am energy spectra obtained from the the dynode pulse height analysis without and with an applied electric field of 10kV/cm, respectively. As can be seen from Fig. 10 (a), the energy spectrum is well represented by a quasi-Gaussian distribution with a FWHM of 13%. This energy resolution is comparable with previous values reported. By comparing Fig. 10 (a) with Fig. 10 (b), it can be seen the peak location is slightly decreased when an electric field is applied because the external electric field partially prevents electrons from recombining with the molecular ions as we explained before.

The number of scintillation photons available to the photomultiplier is an important information in designing the final prototype of liquid xenon imaging chamber. By measuring the single photoelectron peak of the UV photomultiplier with the pulse height analyzer, it is possible to estimate the number of photoelectrons, $N_{\rm pe}$, released from the photocathode of the photomultiplier by the arriving scintillation photons. The estimated value of $N_{\rm pe}$ is about 250 photoelectrons for the spectrum shown in Fig. 10 (a). Assuming that the width of the energy spectrum is mainly determined by the statistical fluctuation of $N_{\rm pe}$, one could also estimate $N_{\rm pe}$ by using the relation $N_{\rm pe} = (2.354/\mathrm{FWHM})^{-2}$, which gives 320 photoelectrons for the same spectrum. Since the photocathode has a quantum efficiency of 15% for the liquid xenon scintillation photons, one could infer that at least 1700 scintillation photons are available to the photomultiplier.

Since the scintillation signal will be the trigger to the readout system of the imaging chamber, the time correlation between the scintillation signal and the charge signal has to be well investigated. Figure 11 (a), (b), and (c) show the ionization signal of the alpha particles, triggered with the photomultiplier anode pulse at the applied electric field of 2.0kV/cm, 3.9kV/cm, and 7.9kV/cm, respectively. Figure 12 (a), (b) and (c) show the ionization signal produced by ^{207}Bi electrons, triggered by the photomultiplier anode pulse at the applied electric field of 0.2kV/cm, 0.5kV/cm and 2.0kV/cm respectively. The leading edge of the charge signal is observed about 2 μsec later than the scintillation pulse. This time difference contains the information on the drift time of the secondary electrons in the liquid xenon.

2.3. Ionization Yield for Electrons and Gamma-Rays in LXe

Excellent energy resolution is a key requirement in the developement of a liquid xenon detector for gamma-ray astrophysics and as part of our investigations we have studied in detail the response of liquid xenon to alpha, beta and gamma radiations.

The dependence of the energy resolution and collected charge on the electric field was measured repeatdly and the results were interpreted using different recombination models. The best energy resolution obtained with fast electrons corresponds to about 4.5% FWHM at 1 MeV. We can explain the large discrepancy between this experimental value and the theoretical Fano limit in terms of recombination fluctuations in the number

of electron-ion pairs associated with the low energy delta electrons. Only under an electric field strength much higher than typically applied would one collect most of the liberated carriers and reach the Fano limited energy resolution. An alternative way to improve the energy resolution of a liquid xenon ionization detector is to complement the charge signal with the scintillation signal associated with recombination. The scintillation signal can be used in two ways, either by directly detecting the light with a photosensitive device such a UV PMT, or by converting the UV photons into free charge carriers via photosensitive dopants.

In the following is a summary of our work in this area. For a more complete description we refer to Aprile *et al.* (1990 (C)).

2.3.1. Energy Resolution Test Chambers

A gridded ionization chamber was used for the measurements with electrons and gamma-rays from a ^{207}Bi source. The cathode and anode were circular stainless steel discs of 6 cm and 4 cm diameter, respectively. The ^{207}Bi source was deposited at the center of the cathode. The grid was made of electroformed Ni mesh stretched on a nickel support ring. The grid had a shieling efficiency of 99%. The grid-cathode separation was about 2.5 mm and the grid-anode separation was about 2 mm. A collection to drift field ratio of 3 was maintained to ensure maximum charge transmission through the grid. Ceramic spacers were used to assemble the electrode structure, suspended from the top flange of a stainless steel vessel. The gas filling,vacuum lines as well as the electrical feedthroughs were all welded on the top flange of the chamber.

The xenon gas was purified with the system previously described.

2.3.2. Energy Resolution of Electrons and Gamma-rays in LXe (^{207}Bi)

The energy spectrum of ^{207}Bi in liquid xenon has been measured repeatedly as a function of electric field strength, in the range (0.06 - 12) kV/cm. Consistent data have been obtained in several experiments, with different chamber geometries and different conditions of the purifiers.

Typical pulse height distributions are shown in Fig. 13. Due to the high detection efficiency of liquid xenon for gamma-rays, the pulse height distribution is dominated by the full energy peaks of the 570 and 1064 keV gamma-ray lines, with a small contribution from the L conversion electrons at 554 and 1048 keV. As the electric field increases, the K-conversion electron lines at 481 and 976 keV can also be observed. In all the spectra, the peak to the right is the calibrating test pulse. Its width indicates the electronic noise contribution. For the data of Fig. 13, the electronic noise was 700 electrons or 15 keV FWHM, approximately constant up to the highest field.

From a least square fit of Gaussian functions to the observed spectral lines, the peaks and widths are obtained at each field setting. For the background a quadratic function is assumed.

The reproducibility of the energy resolution results is very good, as can be seen in Fig. 14, which displays the noise-subtracted energy resolution of the 570 keV line versus electric field, measured by us in four different experiments. For comparison, results in

liquid xenon obtained by other investigators at similar electric fields, are also displayed on the same figure. For this comparison an energy scaling as $E^{-1/2}$ has been used for the data taken with sources other than ^{207}Bi and the published values of the electronic noise have been subtracted.

Most measurements agree reasonably well, strongly suggesting a fundamental process limiting the energy resolution in liquid xenon, independent of chamber geometry and preparation, liquid purity and type of radiation source. This limit is nearly 20 times worse than the Fano factor prediction and approximately 5 times worse than the limit expected from the inverse square law of Possion statistics.

The discrepancy is too large to be explained by effects such as shielding inefficiency of the grid, variation in pulse rise time, or backscattering in the source plate or the liquid. Electron attachment to impurities and trapping by the grid should also be negligible, given the high purity of the xenon and the optimized ratio of collection to drift field typically used. Therefore, we believe that the degradation of the resolution is mostly due to the statistics of charge collection affected by the recombination process.

The two modes of recombination which limit the total charge yield are geminate (Onsager 1938) and columnar (Jaffe 1913, and Kramers 1952).

The basic assumption in the Onsager theory is independent electron-ion pairs, each subject only to the influence of the mutual Coulomb attraction, external field and diffusion. The effect of geminate or initial recombination is best distinguished at low electric fields, if other charge losses due to impurities or bulk recombination can be neglected. The predicted dependence of the collected charge at low electric fields is linear:

$$Q(E) = Q_0 \left[\exp\left(-\frac{r_{kT}}{r_0}\right)\right]\left(1+\frac{E}{E_{kT}}\right) \tag{12}$$

where Q_0 is the charge at infinite field, $\exp(-r_{kT}/r_0)$ is the escape probability in absence of external field E, r_0 is the thermalization length, $r_{kT} = e^2/\epsilon kT$ is the Onsager radius, defined as the distance at which the Coulomb attraction of the ion pair is equal to the thermal energy kT, and $E_{kT}^{-1} = e^3/2\epsilon k^2T^2$ is the slope-to-intercept ratio.

For liquid xenon at a temperature $T = 195$K and with a dielectric constant $\epsilon = 1.75$, the Onsager radius is 490Å and the slope-to-intercept ratio is 1.45×10^{-4} cm/V.

A fit of eq. (12) to our low field ($E < 2$ kV/cm) data is rather poor and yields a much larger value of E_{kT}^{-1}. The reason for the disagreement is probably in the assumption of separated ion pairs which is not valid in liquid xenon. From the average range of 1 MeV electrons in liquid xenon we estimate a mean separation of only 400Å between pairs, which is comparable to r_{kT}, so that electrons which escape geminate recombination with the parent ions may still recombine with other ions. Therefore the application of an external field, which diminishes the average field between each ion and electron in randomly oriented pairs, does not necessarily yield a linear increase of free carriers.

The Jaffe theory of columnar recombination was originally proposed to describe the field effect in dense media subject to heavily ionizing particles, such as alpha particles. It assumes that the electron-ion pairs are distributed in a column of uniform charge density. It also assumes equal electron and ion mobilities, which is not the case in noble liquids. The following equation derived from Jaffe's model in the high field approximation has often

been used to describe the dependence of the collected charge $Q(E)$ on the electric field for minimum ionizing particles:

$$Q(E) = \frac{Q_0}{1 + k/E} \tag{13}$$

where k is the recombination constant and Q_0 is the charge at infinite field.

A fit of this equation to our data, shown in Fig. 15 as a broken line, is also very poor. The best fit values are: $Q_0 = 5.08$ fC and $k = 0.09$ kV/cm, with a χ^2 of 18 per degree of freedom.

The assumption of uniform charge density along the path of the primary ionizing particle is not realistic. It is well known that the rate of energy loss in the liquid increases as the particle slows down and that sudden changes in the ionization rate occur due to delta electrons. To account for the different rate of recombination in the high charge density regions of these delta electrons, we have therefore fitted the data of Fig. 15 with the modified equation:

$$Q(E) = \frac{Q_0 - Q_\delta}{1 + k/E} + \frac{Q_\delta}{1 + k_\delta/E} \tag{14}$$

first used by Bolotnikov *et al.* (1986) to interpret high pressure xenon data, and subsequently used by us and other investigators to interpret ionization data in liquid argon. Here Q_δ is the fraction of charge produced along delta electron tracks and characterized by a recombination constant k_δ, different from the recombination constant k for the primary particle track.

Only delta electrons in a small energy interval will produce sufficiently high ionization densities to require the additional term in eq. (14), since a delta electron with a very low energy cannot produce enough electron-ion pairs, and a delta electron with a very high energy will resemble the primary particle track. The different energies of the delta electrons in this interval would require different Q_δ and k_δ values. Equation (14) is therefore approximate since it uses a weighted average over all energies.

The result of the fit with this equation is shown as a solid line in Fig. 16. The χ^2 is 0.2 per degree of freedom and the values of the fitted parameters are: $Q_0 = 6.04$ fC, $Q_\delta = 1.28$ fC, $k = 0.06$ kV/cm and $k_\delta = 17$ kV/cm. About 22% of the total charge is due to delta electrons, and even at a field $E = k_\delta$ only 50% of this charge would be collected.

We have calculated the number of delta electrons produced in liquid xenon by a 570 keV gamma-ray. Figure 16 shows the rapid increase in energy loss for the region below 50 keV. If we specify a delta electron energy interval between 1 and 20 keV, following the considerations of Miroshinicenko *et al.* (1982), we find that about 150 keV of the primary particle energy is used to produce these delta electrons, consistent with the 22% obtained from our data.

An independent analysis of our data has also been done using the model of Thomas *et al.* (1988). Based on the same argument that the production of delta electrons affects the recombination rate along the ionizing particle track, these authors derived an expression for the field dependence of the collected charge and energy resolution as follows:

$$Q(E) = Q_0 \left[a \frac{\ln(1 + \xi_0)}{\xi_0} + (1 - a) \frac{\ln(1 + \xi_1)}{\xi_1} \right] \tag{15a}$$

$$\text{FWHM}(\%) = \frac{235.5}{\sqrt{E_p}} b \left[\frac{\ln(1+\xi_1)}{\xi_1} - \frac{\ln(1+\xi_0)}{\xi_0} \right] \frac{Q_0}{Q} \qquad (15b)$$

In these equations, the parameter ξ_1 describes the charge density of the minimum ionizing region of the particle track while ξ_0 describes the more heavily ionizing regions of delta electrons, so that $\xi_1 E$ and $\xi_0 E$ have the same meaning as k and k_δ of eq. (14). The parameters a and b of the model are functions of the delta electron minimum and maximum energies, $E1$ and $E2$, and of the energy E_p of the primary particle.

A simultaneous fit of the two equations to our 570 keV low field data is shown in Fig. 17. The χ^2 is 0.3 and the values of the parameters are $Q_0 = 5.1$ fC, $\xi_0 E = 1.8$ kV/cm, $\xi_1 E = 0.05$ kV/cm, $a = 0.2$ and $b = 3.1$. The corresponding values of $E1$ and $E2$ are 14.3 keV and 70.3 keV, respectively, close to the values predicted by Imel and Thomas from the fit of their liquid xenon data, limited to 1.8 kV/cm.

When the same analysis is, however, performed on our entire data set, (Fig. 18), extending up to 10 kV/cm, the functions fit the data less well and the values of the parameters are: $Q_0 = 5.6$ fC, $\xi_1 E = 13.8$ kV/cm, $\xi_0 E = 0.09$ kV/cm, $a = 0.2$ and $b = 1.5$. The corresponding limits for the delta electron energy interval are 4.1 keV and 16.4 keV, close to the estimates of reference.

A good description of both low and high field data is not possible within the framework of the available models, and an improved theory combining some features of the existing ones is needed. The hypothesis that the energy resolution is limited by statistical fluctuations associated with delta electrons seems to be a right step in this direction since it can explain the experimental results in liquid argon and xenon ionization chambers.

4. REFERENCES

E. Aprile, R. Mukherjee and M. Suzuki, "Measurements of the Lifetime of Conduction Electrons in Liquid Xenon," accepted for publication in *Nucl. Instr. and Meth. A*, **300**, (1991) (A).

E. Aprile, R. Mukherjee and M. Suzuki, *IEEE Trans. in Nucl. Sci.*, NS-37 No. 2 (1990) 553 (B).

E. Aprile, R. Mukherjee and M. Suzuki, "Performance of a Liquid Xenon Ionization Chamber Irradiated with Electrons and Gamma-Rays," *Nucl. Instr. and Meth. A*, **A 302** (1991), 177 (C).

G. Bakale, U. Sowada and W. F. Schmidt, *J. Phys. Chem.*, Vol. 80, No. 23 (1976) 2556.

A. E. Bolotnikov *et al.*, *Pri. Tekh. Eks.*, **4**, (1986) 42.

G. Jaffe, *Ann. Physik*, **42**, (1913) 303.

H. A. Kramers, *Physica*, **18**, (1952) 665.

S. Kubota, M. Hishida, M. Suzuki and J. Ruan(Gen), *Nucl. Instr. and Meth.*, **196**, (1982) 101.

V. P. Miroshinicenko, P. L. Newskij and B. U. Rodinov, "Elementary Particles and Cosmic Rays," Moskow, Energoisdat 1982, translated by W. Schmidt.

L. Onsager, *Phys. Rev.*, **54**, (1938) 554.

J. Thomas, D. A. Imel and S. Biller, *Phys. Rev. A*, **38**, (1988) 5793.

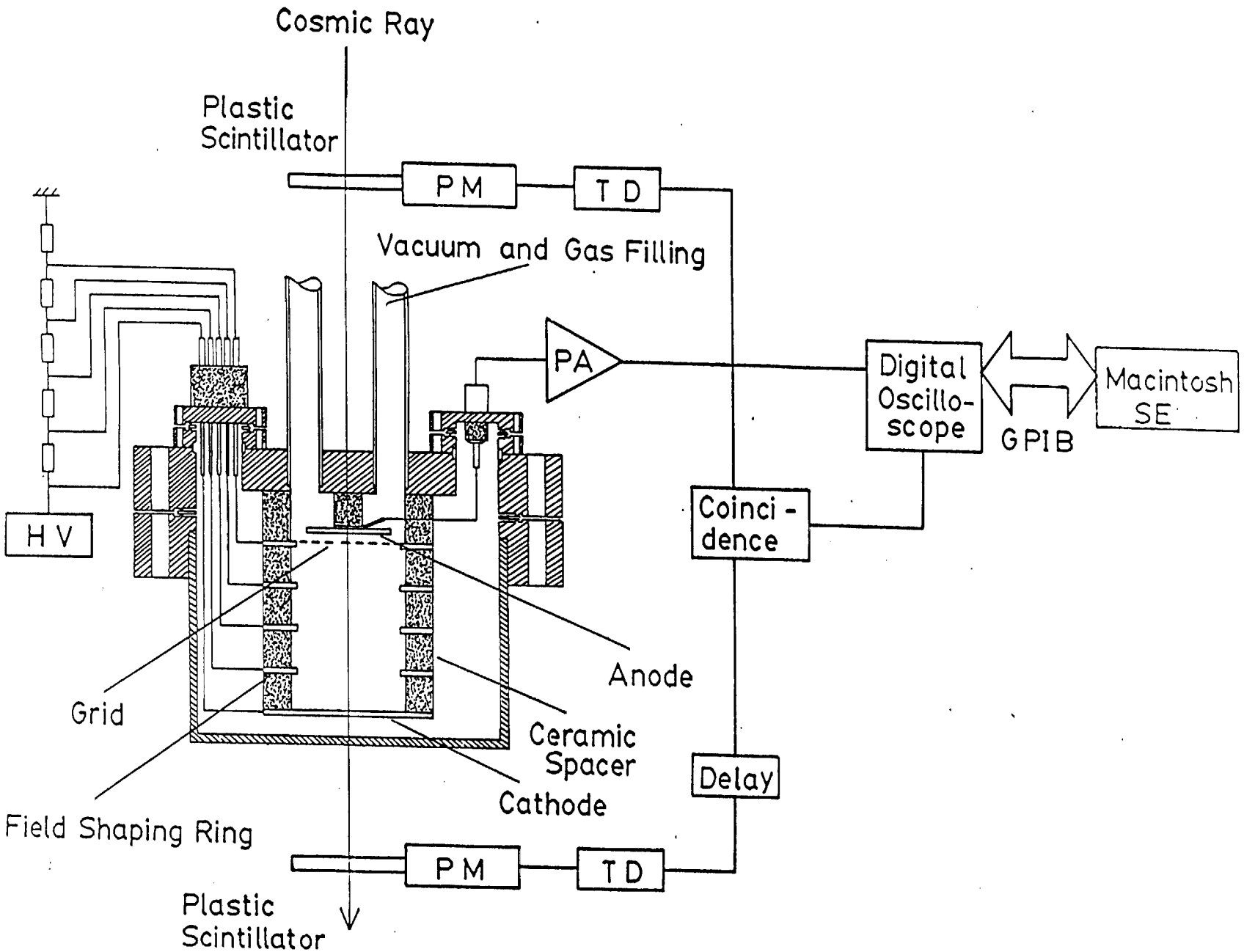

Fig. 1. Schematic of the gridded ionization chamber, cosmic ray trigger and the associated electronics for the electron lifetime measurements.

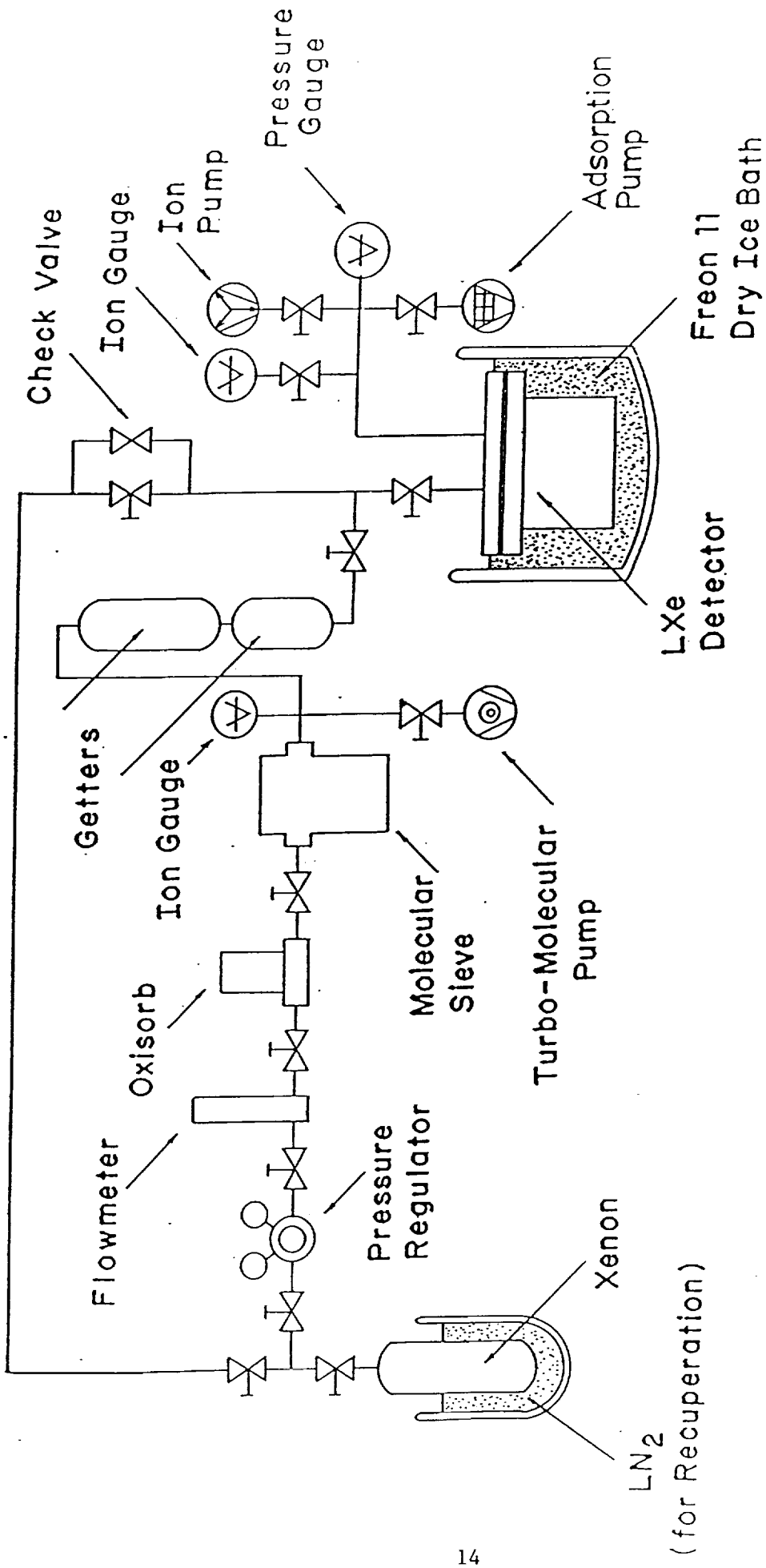

Fig. 2. Schematic of the liquid xenon purification system.

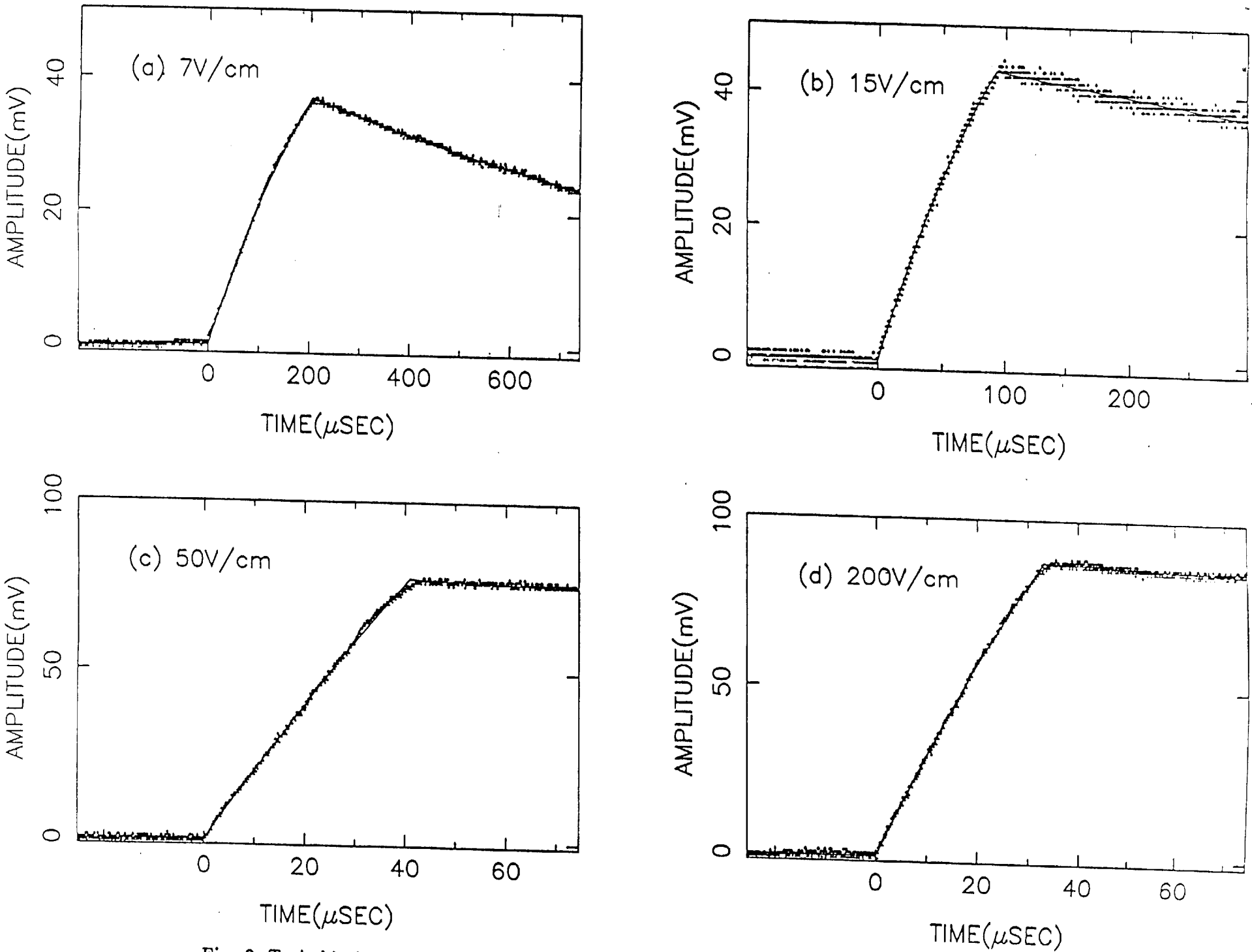

Fig. 3. Typical ionization signals generated by cosmic ray tracks in liquid xenon at different electric fields. The solid curves are the results of the fit with the theoretical pulse shapes.

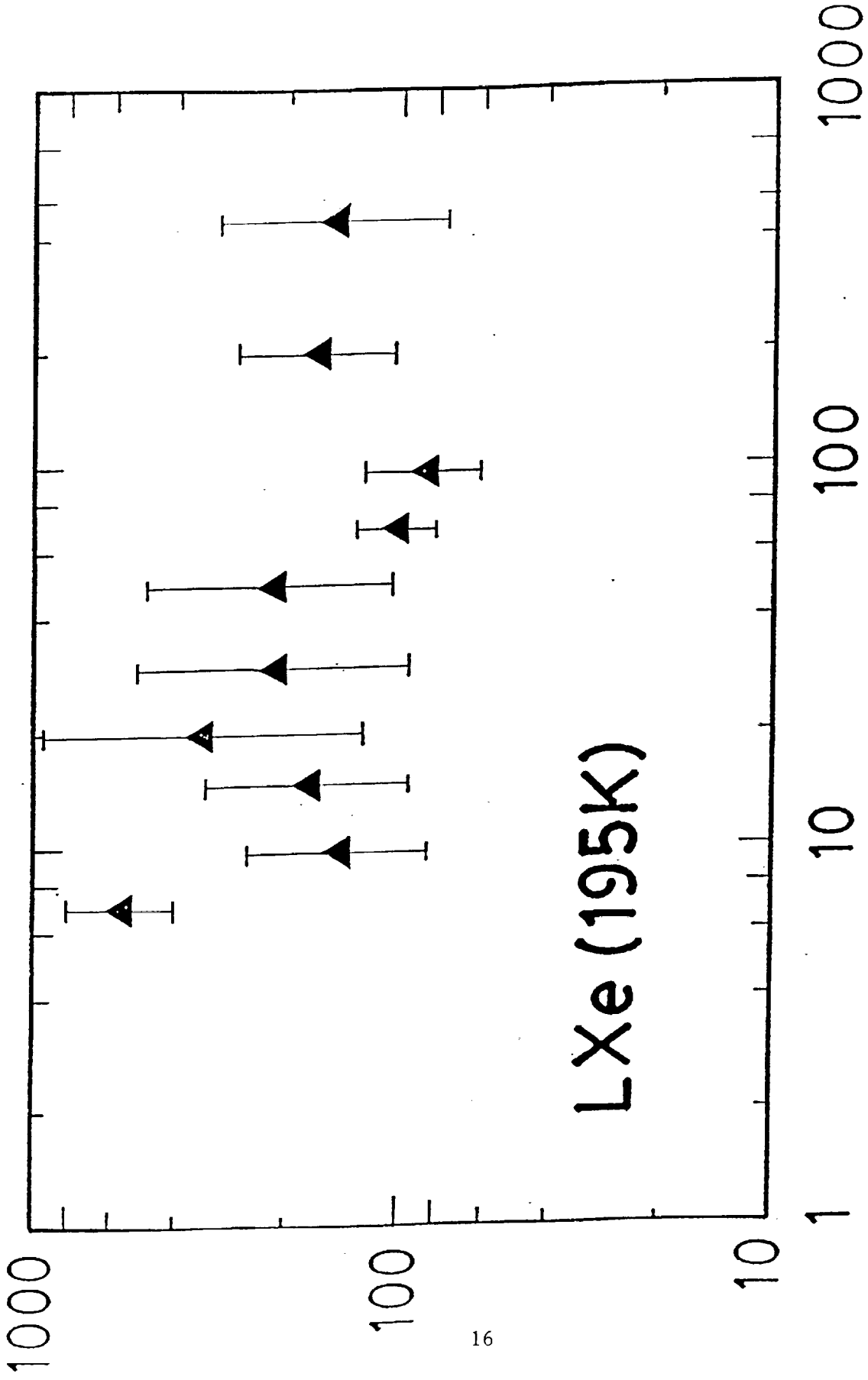

Fig. 4. Electric field dependence of the average electron lifetime in liquid xenon at $T = 195$ K.

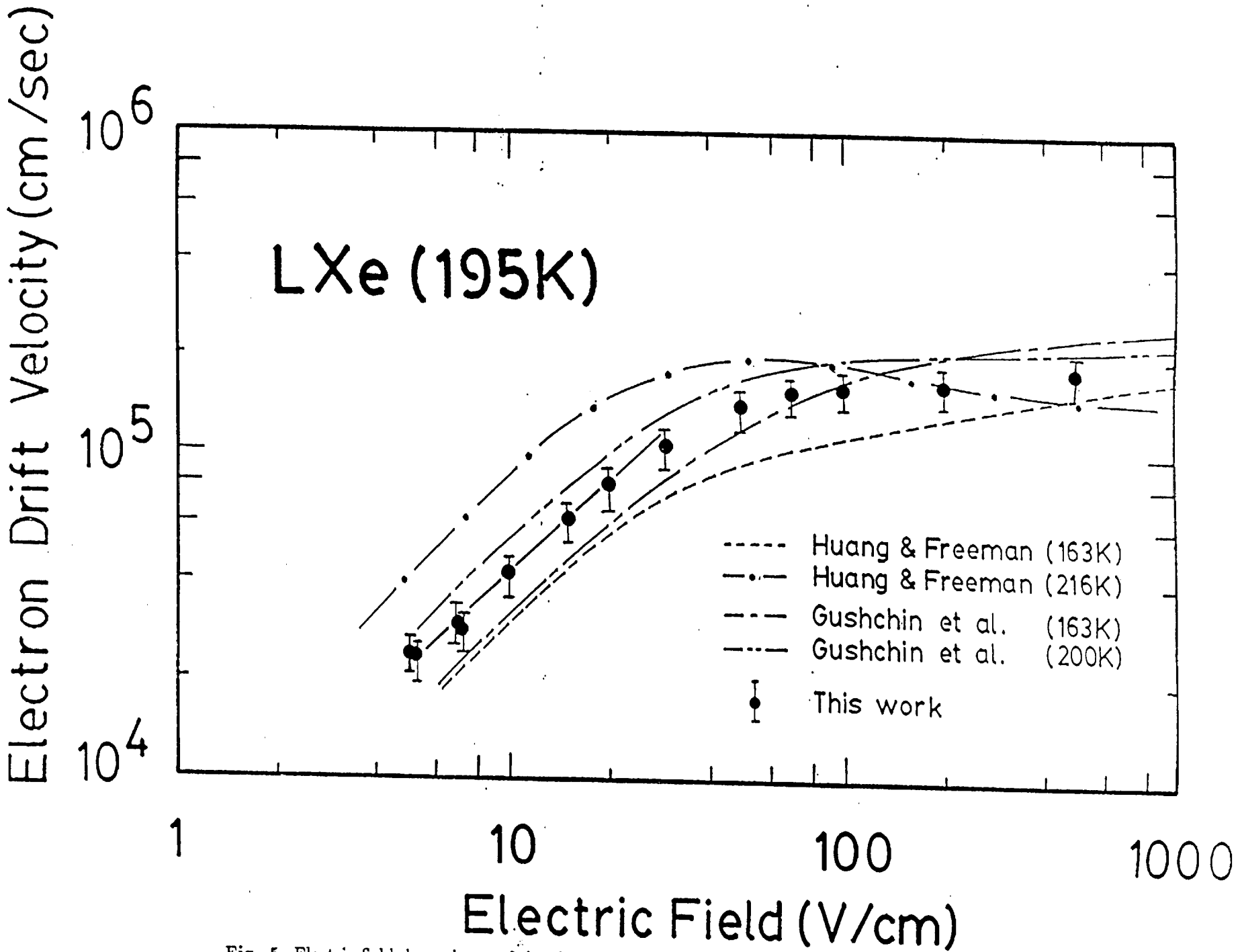

Fig. 5. Electric field dependence of the electron drift velocity in liquid xenon at $T = 195$ K. The solid line is the fit of $v_d = \mu_0 E$, giving $\mu_0 = 4230 \pm \text{cm}^2\text{V}^{-1}\text{s}^{-1}$. The other lines are the data of other investigators.

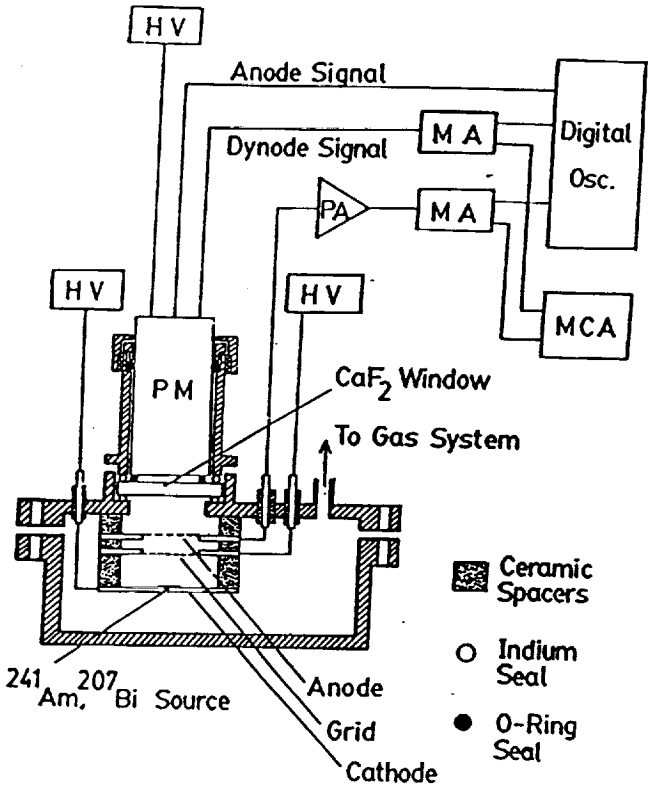

Fig. 6. Schematic of the ionization chamber and the associated electronics for the liquid xenon scintillation experiments.

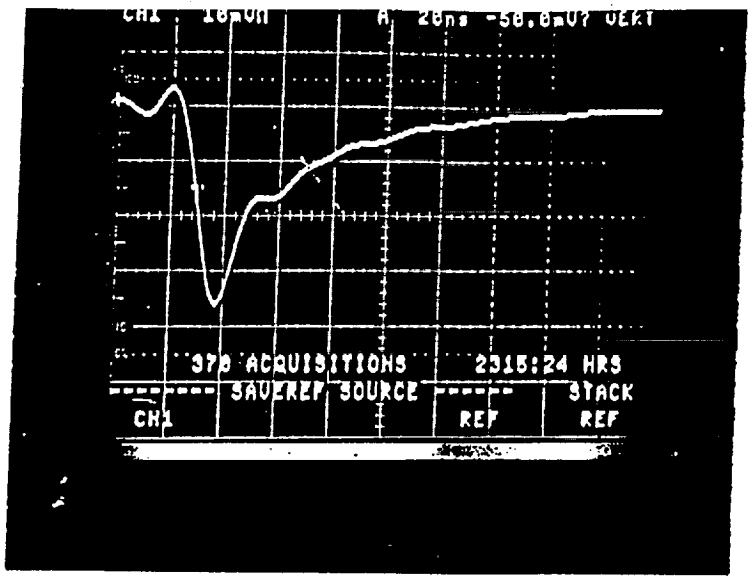

(a)

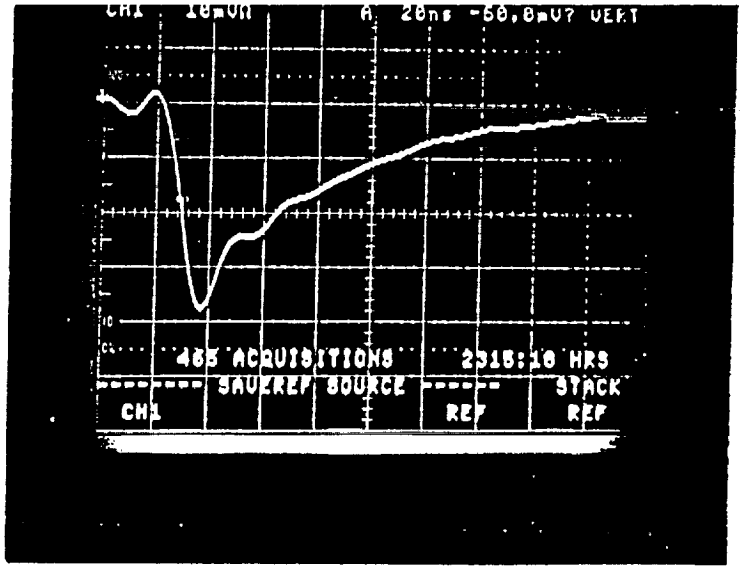

(b)

Fig. 7. Scintillation light of ^{207}Bi conversion electrons in liquid xenon (a) without and (b) with an applied electric field of 2 kV/cm (10 mV/div., 20 nsec/div.).

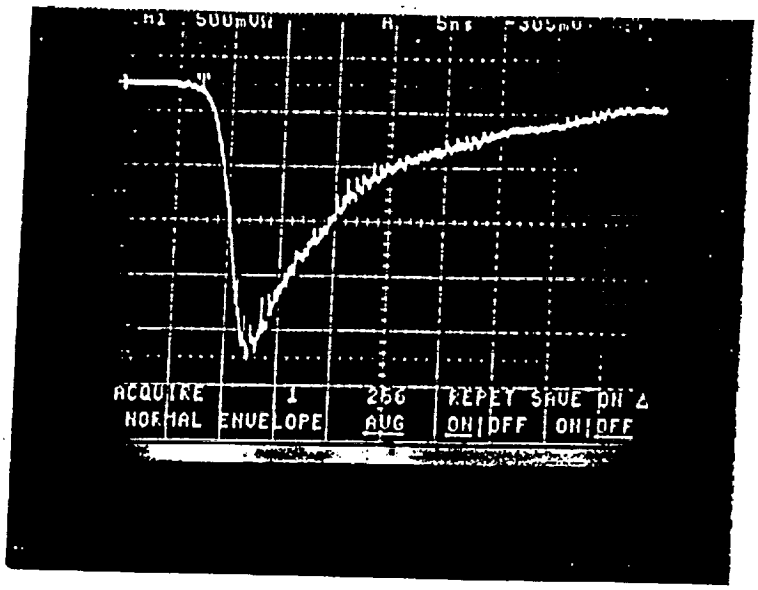

(a)

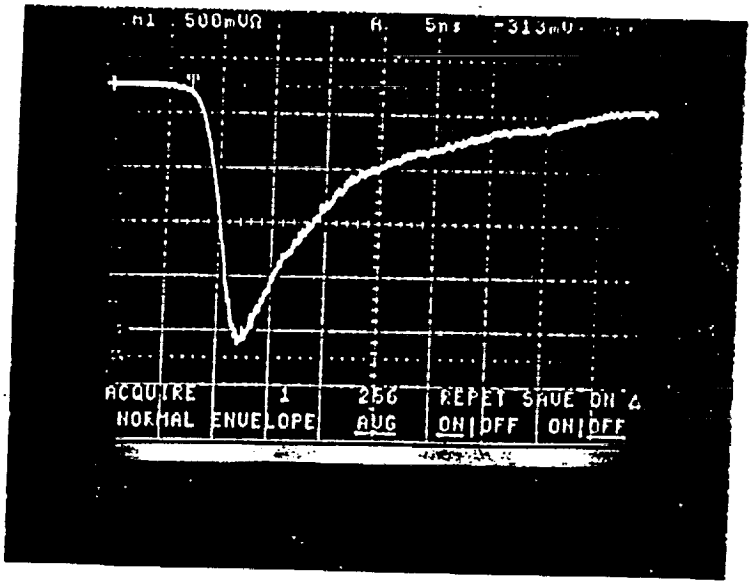

(b)

Fig. 8. Scintillation light of ^{241}Am alpha particles in liquid xenon (a) without and (b) with an applied electric field of 7.9 kV/cm (500 mV/div., 5 nsec/div.).

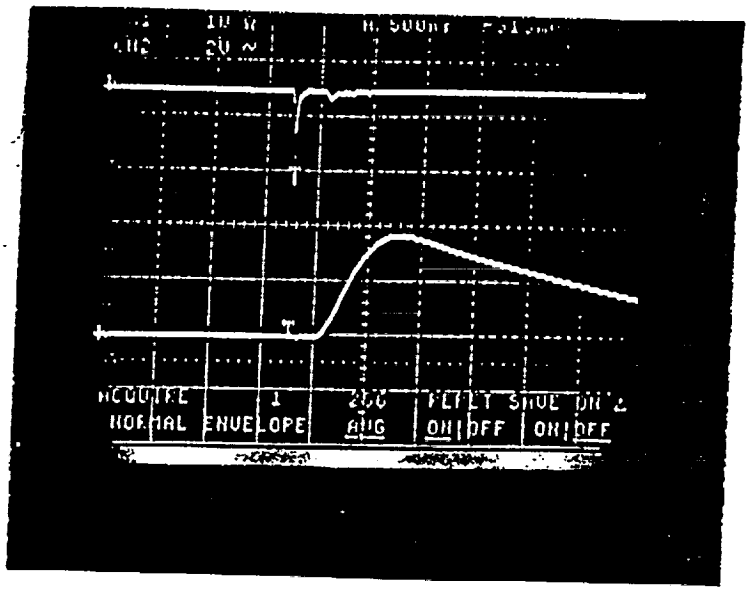

Fig. 9. Integrated dynode pulse (lower trace: 2V/div., 500 nsec/div.) triggered by the anode pulse of the photomultiplier (upper trace: 1V/div., 500 nsec/div.), alpha particles.

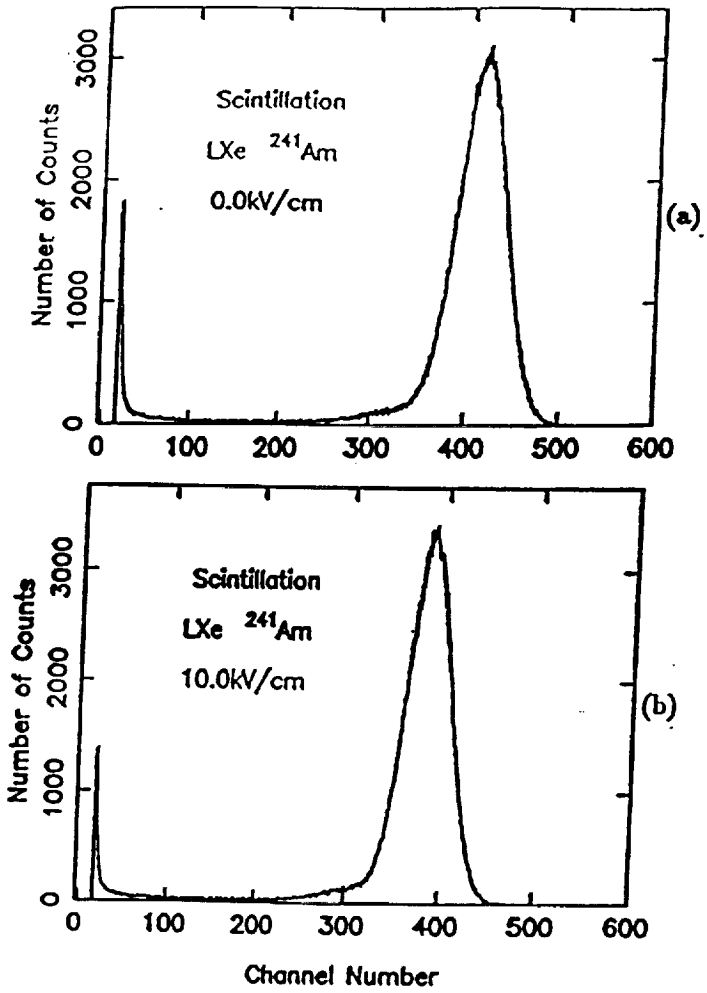

Fig. 10. ^{241}Am energy spectrum obtained from the scintillation in liquid xenon (a) without and (b) with an applied electric field of 10 kV/cm.

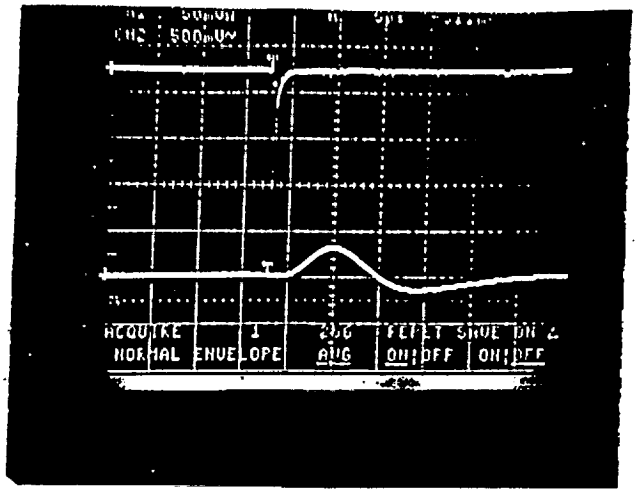

(a)

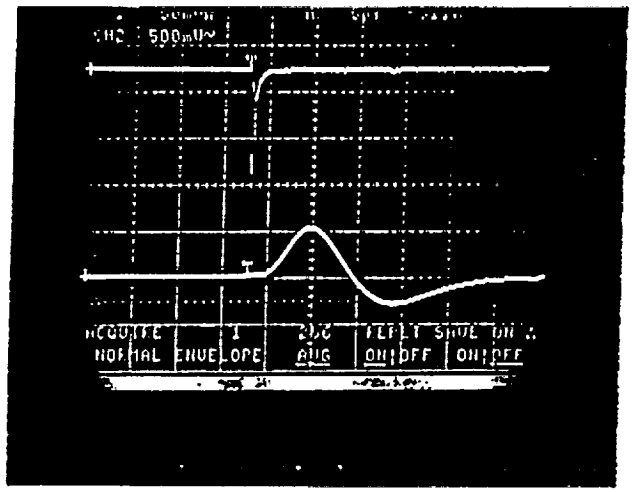

(b)

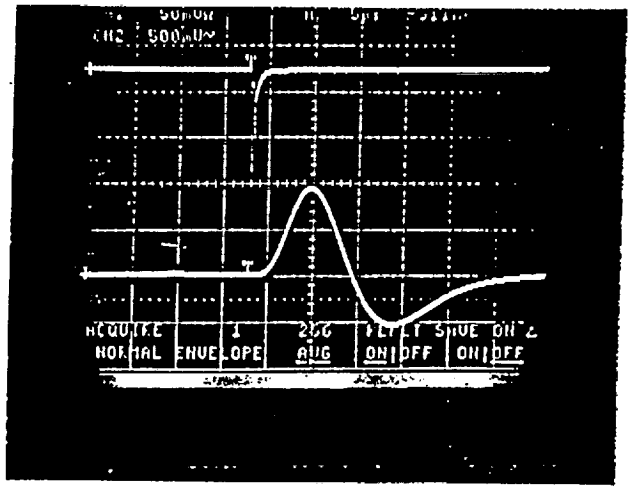

(c)

Fig. 11. ^{241}Am alpha particle ionization signals (lower trace: 500 mV/div., 5 microsec/div.) at an applied electric field of (a) 2.0 kV/cm, (b) 3.9 kV/cm and (c) 7.9 kV/cm.

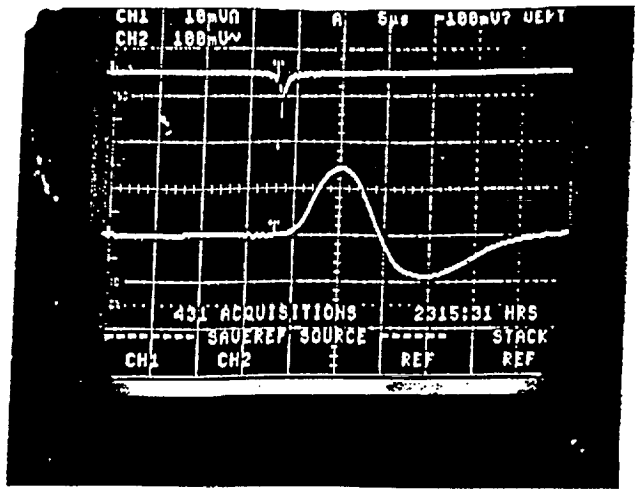

(a)

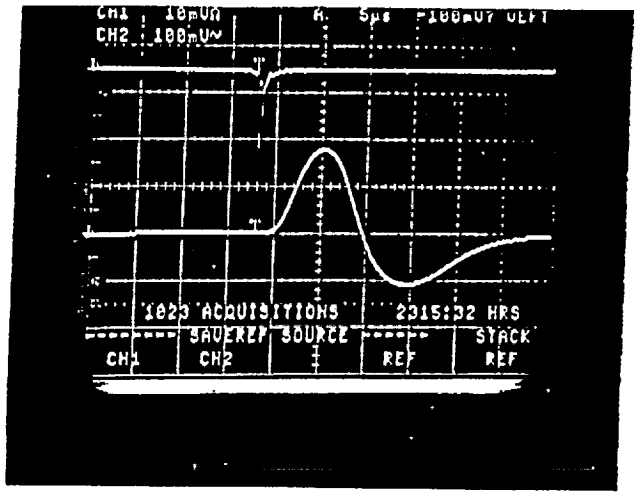

(b)

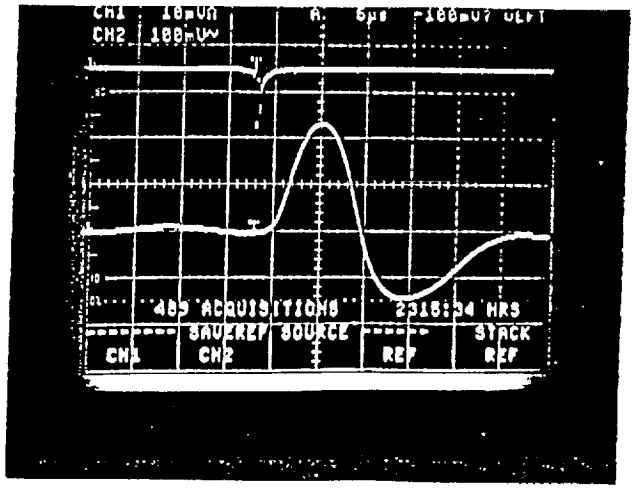

(c)

Fig. 12. ^{207}Bi conversion electrons ionization signals (lower trace: 100 mV/div., 5 microsec/div.) at an applied electric field of (a) 0.2 kV/cm, (b) 0.5 kV/cm and (c) 2.0 kV/cm.

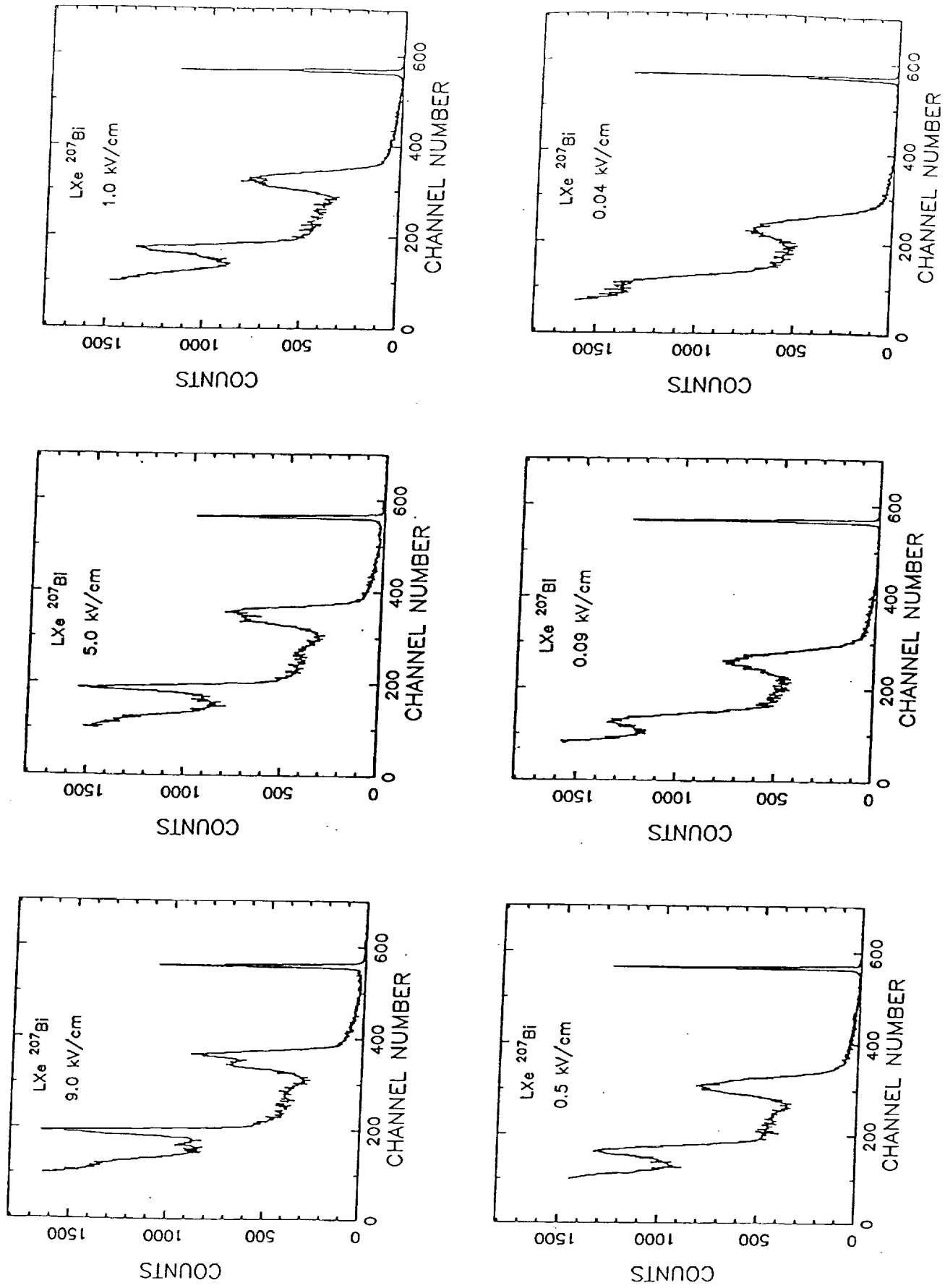

Fig. 13. ^{207}Bi pulse height distributions in liquid xenon at six different electric fields. The FWHM of the test pulse distribution (rightmost peak) is 15 keV.

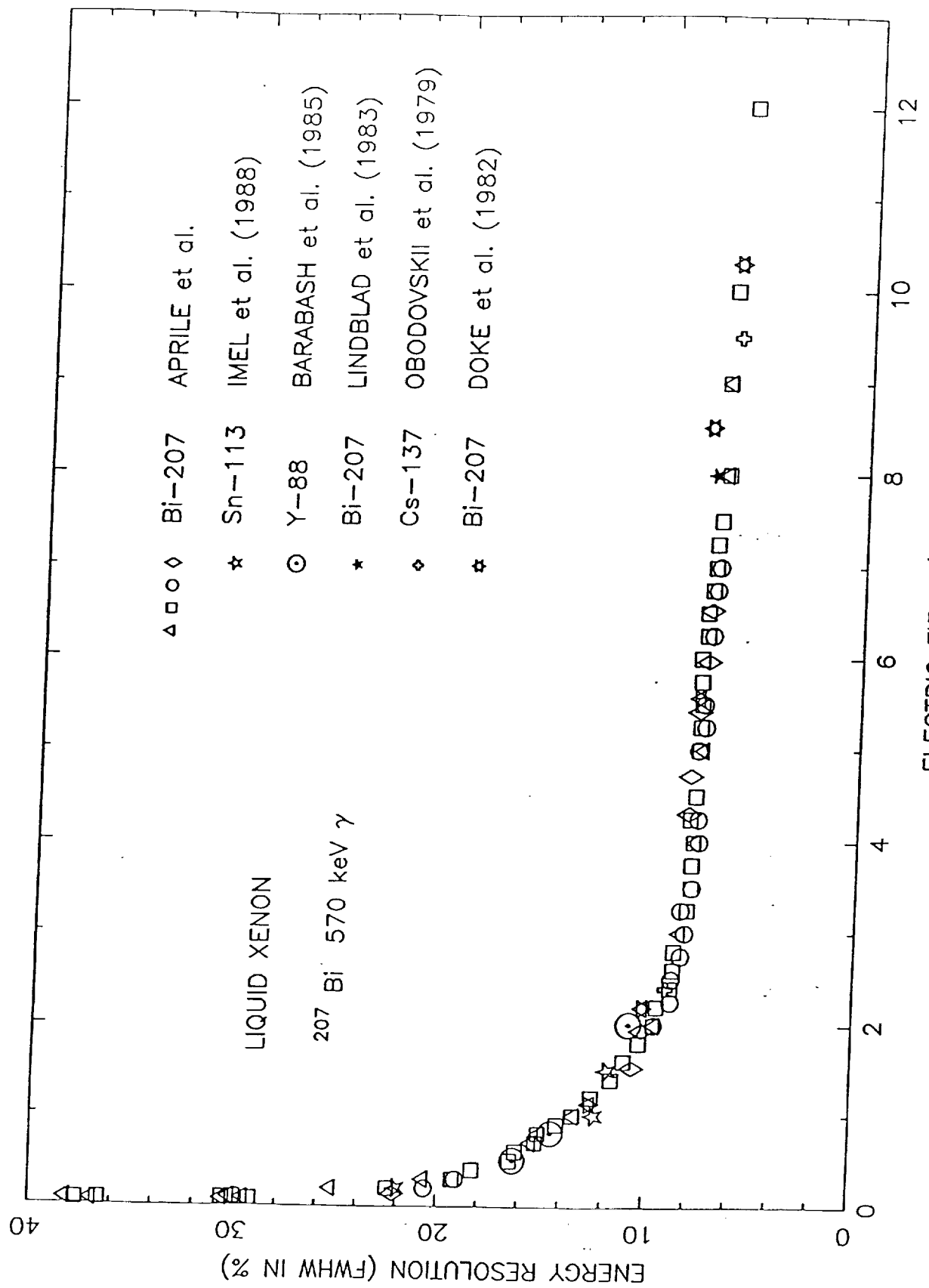

Fig. 14. Noise subtracted energy resolution of 570 keV gamma-rays vs. applied electric field. For comparison, results of other investigators are also shown.

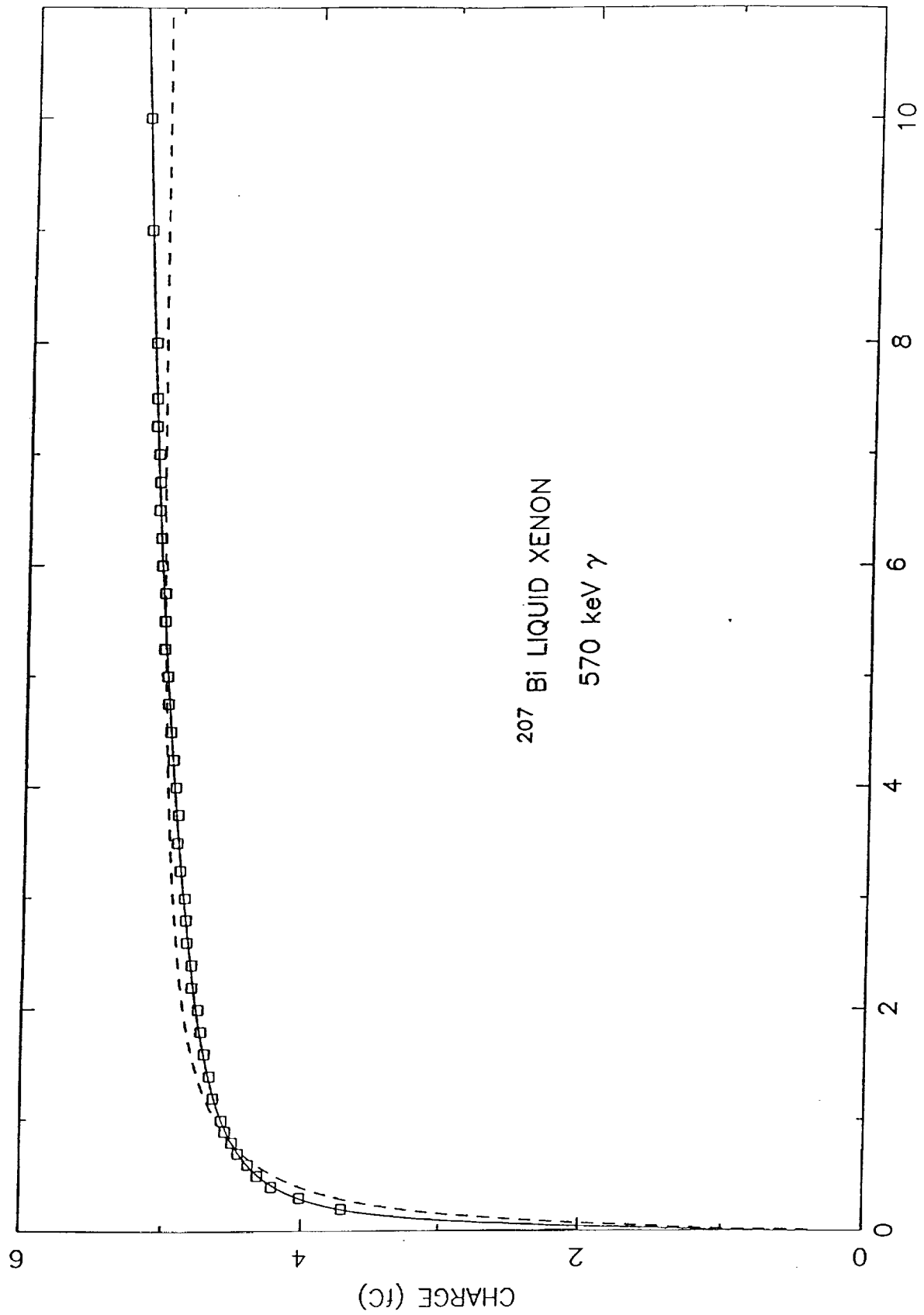

Fig. 15. Collected charge as a function of applied electric field for 570 keV gamma-rays. Fits of equations (13) and (14) are shown as a broken and a solid line, respectively.

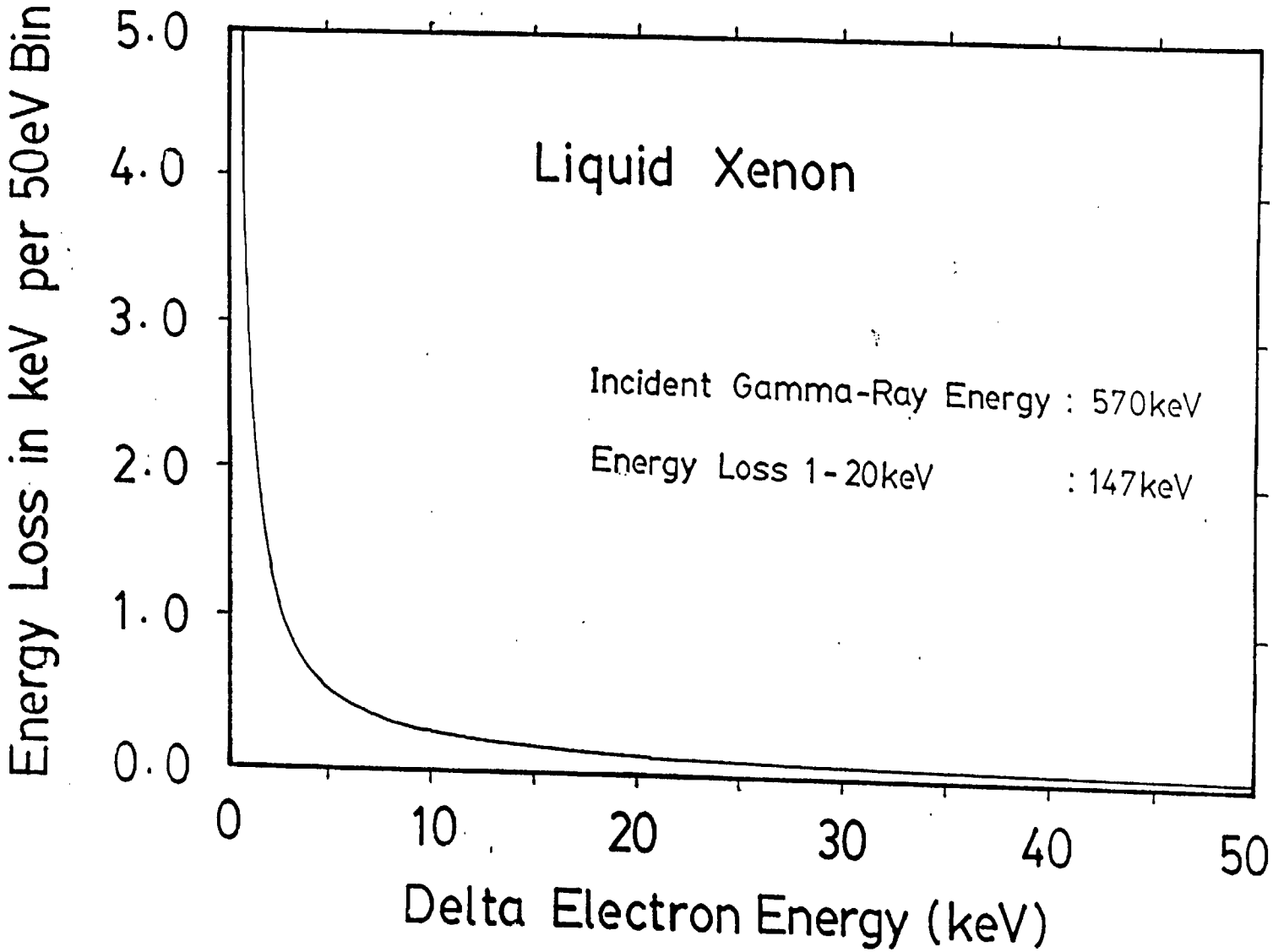

Fig. 16. Energy loss of 570 keV phoelectrons in liquid xenon for the production of delta electrons with energies below 50 keV.

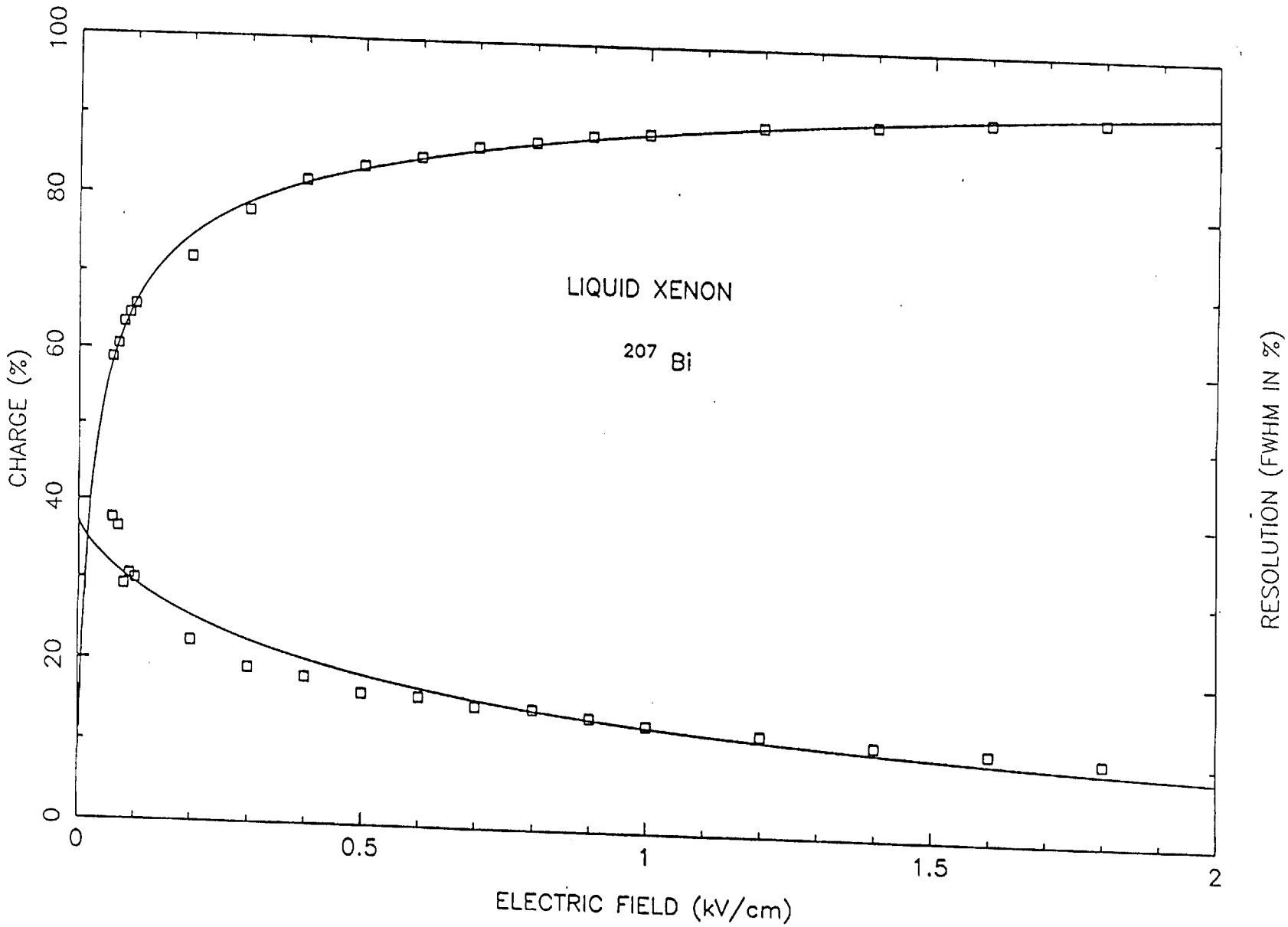

Fig. 17. A simultaneos fit of equations (15a) and (15b) to the collected charge and energy resolution of 570 keV gamma-rays, for electric fields lower than 2 kV/cm.

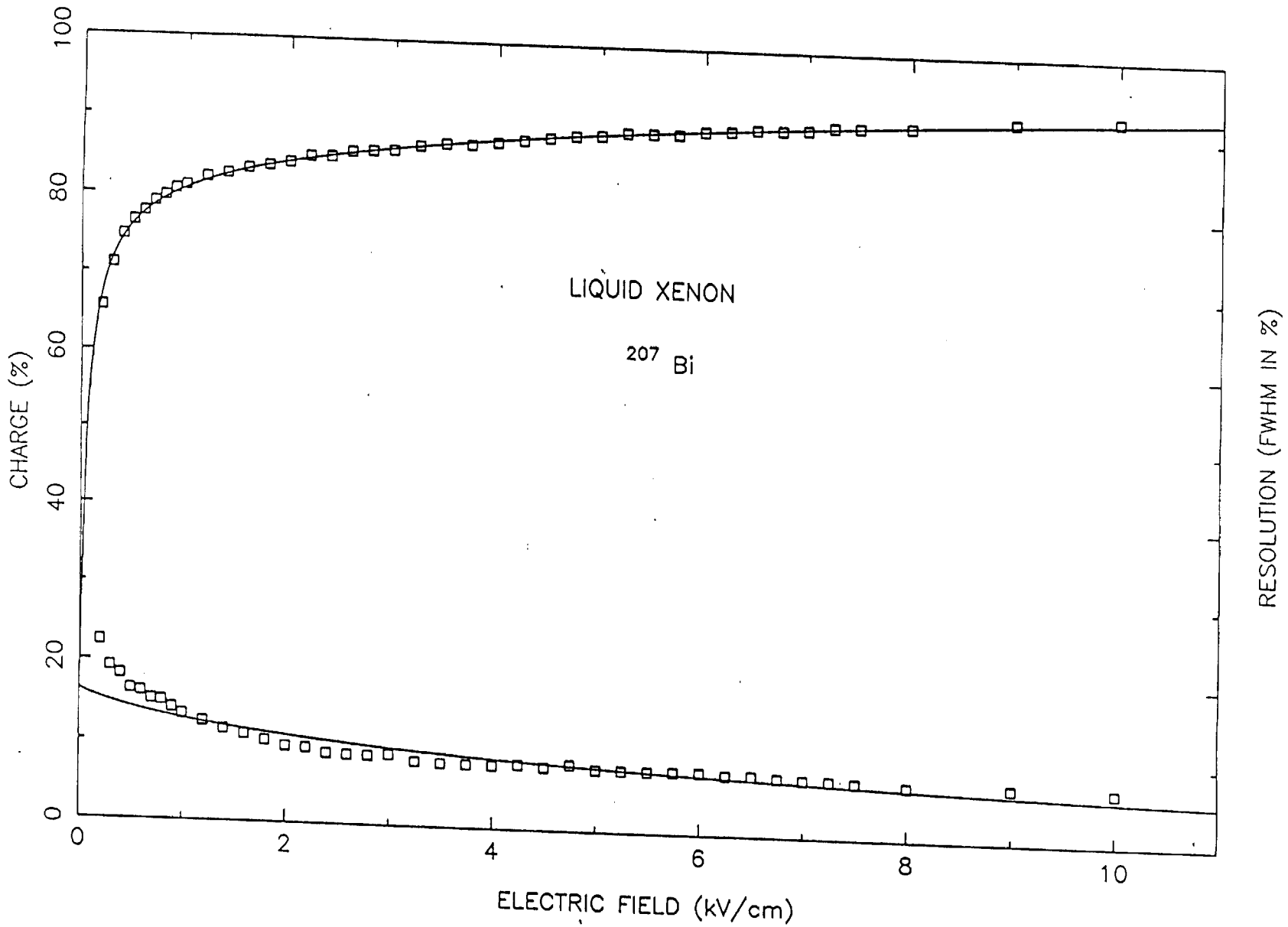

Fig. 18. A simultaneos fit of equations (15a) and (15b) to the collected charge and energy resolution of 570 keV gamma-rays, for electric fields lower than 10 kV/cm.